Anal. Bioanal. Electrochem., Vol. 16, No. 1, 2024,23-48
https://www.doi.org/10.22034/abec.2024.710593

Analytical & Bioanalytical Electrochemistry

Full Paper

Synthesis of TiO_2@Multi-Walled Carbon Nanotube/Graphene Oxide Nanocomposite Electrode for Boosting Electrochemical Detection of Traces Azithromycin in Biological Samples

Jallal Zoubir,* Ali Assabbane, and Idriss Bakas

Team of Catalysis and Environment, Ibn Zohr University, Faculty of Sciences, BP 8106, Agadir, Morocco

*Corresponding Author, Tel.: +212606800735
E-Mail: zoubirjallal@yahoo.fr

Received: 15 June 2023 / Accept with minor revision: 27 January 2023 /
Published online: 31 January 2024

Abstract- Voltammetric detection of active substances has occupied an important place in the last decades. In this study, a novel highly efficient electrochemical sensor was fabricated using a combination of titanium dioxide nanoparticles and multi-walled carbon nanotubes mixed with graphene oxide sheets for the sensitive detection of the antibiotic Azithromycin. The results show that the constructed electrode has excellent electrocatalytic activity for Azithromycin detection (pH 7) compared to the unmodified electrode due to the mobilized TiO_2 nano-conductors on the MWCNTs@GO. The electrochemical behavior of Azithromycin was perfectly reversible. Transmission electron microscopy, X-ray diffraction, infrared spectroscopy, and Raman spectroscopy analyses were performed to examine the particularities of the IL-TiO_2 NPs@MWCNTs/GO/GCE interface. The effects of pH, accumulation time, scan rate, and the amount of multi-walled carbon nanotubes required for creation were investigated and optimized by applying Cyclic Voltammetry and DPV at pH 7.0. Phosphate buffer medium. The results showed that the number of protons and electrons involved in the electrooxidation reaction of Azithromycin is equal. The calibration curve was plotted in the concentration range of 10^{-3} to 0.5×10^{-6} M using the DPV method. The limit of detection and limit of quantification were calculated as 1.772×10^{-8} M and 5.83×10^{-8} M, respectively. The described method was applied to determine Azithromycin in pharmaceutical formulations and human blood and urine samples. The good recovery values between 96.6% and 99.1% suggest the applicability, efficiency, and reliability of the sensor for the determination of Azithromycin.

Keywords- Azithromycin; Sensor; IL-TiO_2 NPs@MWCNTs/GO/GCE; Human serum

1. INTRODUCTION

Azithromycin was mentioned for usage during the Covid-19 pandemic, particularly in conjunction with hydroxychloroquine (HCQ), for the treatment of SARS-CoV-2. After a French study by Gautret et all [1–4]. Titled "Hydroxychloroquine and azithromycin as a treatment of COVID-19: results of an open-label non-randomized clinical trial: conclusions of an open-label non-randomized clinical trial" which was published in 2020, on Azithromycin, attention was drawn to it. However, the study has received harsh criticism, especially with regard to the effect of bringing the viral load of patients with the disease to zero. Since then, hospitals have been using these medications in COVID-19 patient clinical studies, especially in Brazil (BRASIL, 2020) [5–7]. The primary function of AZT is bacteriostatic, meaning it works to stop bacterial growth. Y, several studies show that macrolides have anti-inflammatory and antiviral effects in addition to their antibacterial activity, making them one of the immunomodulatory medicines of action in a variety of respiratory disorders [8–14]. There is a growing need for stronger analytical methods in the context of this research to identify and/or quantify one or more components in a substance sample, particularly for substances with known or potential effects on human health as a result of the growing number of environmental pollutants[11,15]; sensors have been developed: For the voltammetric detection of the antibiotic azithromycin in biological samples, use sensor IL-TiO_2-NPs@MWCNTs/GCE. A novel macrolide antibiotic named azithromycin (N-methyl-9a-aza-9-deoxo-9-dihydro-9ahomoerythromycin A, or AZT) is used to treat or prevent several bacterial infections like sinusitis, pneumonia, typhoid, pneumonia, ear infections, and strep throat [16,17]. By inducing a number of problems in the bacteria, this medication stops their survival and growth. The majority of azithromycin that is ingested is eliminated unaltered through urine. Antibiotic overuse causes bacterial strains to become resistant to them, as well as allergic responses, liver damage, yellowing of the teeth, and digestive problems [16,18,19]. Also, it results in the transmission of genes that are resistant to antibiotics and may result in cancer in people who eat foods derived from animals that have been tainted with antibiotics. Semi-synthetic erythromycin derivative and 15-cyclic lactone antibiotic, Azithromycin [20]. Treatment for respiratory tract infections, toxoplasmosis, and non-classical pathogens such Helicobacter pylori, pediatric infections, and opportunistic infections in AIDS are all greatly aided by azithromycin [21–23]. Azithromycin has been used to treat a number of sexually transmitted diseases, skin and soft tissue infections, and respiratory infections[18,20,24,25]. This drug is marketed on the open market in capsule and compound tablet form, all of which can be excreted in the urine. It is very rapidly absorbed when given orally in syrup or tablet form [24]. Several analytical methods have already been reported for the qualitative and quantitative analysis of the antibiotic Azithromycin. Among these methods, we can mention high performance liquid chromatography (HPLC) [26], HPLC–mass spectrometry [27], liquid chromatography (LC) [20,28], microbiological assays [29], liquid chromatography–mass spectrometry(LC–MS)

[30], and spectrophotometric methods [25,31]. Traditional methods require expensive equipment and are not readily available in many laboratories, whereas electrochemical studies use different modified electrodes [32–34]. Compared to other methods, electroanalytical methods require inexpensive instrumentation, take less time and are more efficient, require less solvent, and do not require any sample pretreatment procedures [35–38]. the electrochemical determination of Azithromycin on glassy carbon [24,39], graphite [40] , Azithromycin electrochemical detection using a molecularly imprinted polymer prepared on a disposable screen-printed electrode [14], Electrochemical behavior of azithromycin at graphene and ionic liquid composite film modified electrode (Gr/IL/GCE) [17], Facile synthesis of the necklace-like graphene oxide-multi-walled carbon nanotube nanohybrid and its application in electrochemical sensing of Azithromycin (GO-MWCNTs/ GCE) [41], An azithromycin electrochemical sensor based on an aniline MIP film electropolymerized on a gold nano urchins/graphene oxide modified glassy carbon electrode (MIP-GNU/GO/PANI) [24], A sensitive and selective voltammetric sensor based on multiwall carbon nanotubes decorated with $MgCr_2O_4$ for the determination of azithromycin ($MgCr_2O_4$- MWCNTs/GCE**)** [20], A study of the catalytic role of a gold electrode in the electrochemical activation of four macrolide antibiotics in sodium bicarbonate solution ,Bare gold electrode [42] have been frequently published**.** The creation of new measurement tools to provide better chemical information we have the immobilization of nanomaterials on the surface of the working electrode has had a very strong impact on the sensor because of the considerable progress made in the preparation of nanoparticles of variable and controllable shape. In this sense, multiwall carbon nanotubes (MWCNTs) have attracted considerable interest from the current team due to their large surface area, special electronic characteristics, high chemical stability and conductivity[43,44]. As an electrode material, they facilitate electron exchange between the sensor and the target molecule and provide a new surface for the design of a novel modification-based sensing device [44–46]. The modification of the sensing surface by mobilizing the ionic liquid from the doped IL-TiO_2-NPs titanium dioxide nanoparticles provides a conductive surface for sensing electrodes. conductive surface for sensing electroactive and bioactive molecules[47]. The uniform layer of IL-TiO_2-NPs formed on the electrode surface directs the charge transfer and leads to the formation of electron transfer channels between the active centers and the electrode surface. These modified electrode surfaces offer electrocatalytic and antifouling properties. They also prevent unwanted reactions with the active interface of the fabricated electrode [48–50]. We chose to use the conbianaision between multiwall carbon nanotubes (MWCNTs) with graphene oxide sheets to mobilize titanium dioxide nanoparticles to form a nanocomposite note IL-TiO_2-NPs@MWCNTs/Graphene Oxide [51], which combines the high charge density of IL-TiO_2-nano and superior active surface area with multiwall carbon nanotubes (MWCNTs) and graphene oxide sheets to achieve maximum edge density per unit area.

In this research, a novel highly efficient electrochemical sensor IL-TiO_2-NPs@MWCNTs/Graphene Oxide/GCE was fabricated using a combination of titanium dioxide (TiO_2) nanoparticles, multi-walled carbon nanotubes (MWCNTs), and graphene oxide (GO) sheets for the voltammetric determination of the antibiotic Azithromycin. Structural and electrochemical characterizations of IL-TiO_2-NPs@MWCNTs/GO/GCE revealed that it has excellent electrical properties as well as a large active surface area compared to the MWCNTs/GCE multiwall carbon nanotube paste electrode. The main experimental parameters influencing the determination of Azithromycin antibiotic were studied and optimized under the optimized experimental conditions. The performance characteristics of the developed IL-TiO_2-NPs@MWCNTs/graphene oxide/GCE sensors were discussed in detail. The sensors were successfully applied for the determination of the antibiotic Azithromycin in pure form, pharmaceutical preparations and real samples such as human urine and blood; the results obtained are in good agreement with those obtained by the official method.

2. EXPERIMENTAL SECTION

2.1. Chemicals

Azithromycin antibiotic and multiwall carbon nanotubes (D.O. 6-9 nm, 95% Carbon) were purchased from Sigma Aldrich (Durban, RSA). The following chemicals were purchased from Merck (Darmstadt, Germany): urea, titanium tetrachloride, N, N-dimethyl formamide, hydrochloric acid, sodium hydroxide, dibasic sodium phosphate, and monobasic sodium phosphate; carbon graphite was obtained from Sigma-Aldrich (Steinheim, Germany). Analytical grade chemicals were used throughout. By combining conventional Na_2HPO_4 and NaH_2PO_4 solutions at various pH levels, phosphate buffer solutions (PBS) of 0.2 M were created. In solutions of 0.2 M phosphate buffer, azithromycin was dissolved (PBS). Fluka produced potassium hexacyanoferrate III $K_3Fe(CN)_6$ and potassium hexacyanoferrate IV $K_3Fe(CN)_6$. Daily, an adequate dilution of the stock solution was used to create the test standard solutions.

2.2. Instrumentation

For measuring pH, a digital pH meter (model CRISON micro pH 2000) with a 0.1 precision was employed. On a 797VA computerized system (Origalys Electro Chem SAS type Potentionstat/galvanostat with a standard three electrode system), all electrochemical experiments were carried out. The working electrode was either a pure glassy carbon electrode (GCE) or a modified IL-TiO_2-NPs@MWCNTs/GCE electrode, while the reference electrode was a saturated Ag/AgCl (3 M KCl) electrode and the auxiliary electrode was a platinum wire electrode. A five-wall, three-electrode electrochemical cell, an Origalys Electro Chem SAS Potentionstat/galvanostat, driven by Origa-mastre 5 software installed in a personal computer,

is used to process the obtained data. The SEM JEOL at the University Ibn Zohr of Agadir, Morocco, has images of all the pastes we have created for various studies. The X-ray spectra from the University Ibn Zohr of Agadir, Morocco, were acquired using the X-ray diffractometer PERT-PRO (BRUKER-AXS) with CuK radiation (λ_{Cu}=1.5406Â), which is placed at the research center. This allowed the chemical composition of the various pastes we developed to be analyzed. The steps in the diffraction angles (2) were 0.02 degrees, ranging from 10 to 100 degrees.

2.3. Synthesis of TiO_2NPs

TiO_2-NPs were synthesized by modifying the co-precipitation technique by adding 25 mL of $TiCl_4$ to 100 mL of deionized water in an ice bath [22]. Similar to this, 200 mL of deionized water was used to dissolve 20 g of urea. The urea solution was then gradually added to the $TiCl_4$ contents, which were then heated for around 120 minutes at 160 ºC on a hot plate using a magnetic stirrer. After the reaction was complete, a white colloidal solution was created. The colloidal solution was centrifuged with rotary centrifugal force at 1400 rpm for 10 minutes. The product was centrifuged, the leftover material was cleansed with deionized water several times, and then it was dried for three hours at 80°C.

2.4. Ionic Liquid Functionalization for IL-TiO_2-NPs

Similar to the earlier method [23] with a simple modification, 20 mg of TiO_2-NPs were distributed in 5 mL of methanol and ultrasonified for 3 hours. For ultra-sonification, the preceding mixture was then blended with 15 mL of trihexyltetradecylphosphonium ionic liquid and left for 6 hours at 50 °C. The precipitate was filtered and thoroughly washed with deionized water after the mixture was put into a 50 mL beaker. After being dried at 100 °C, the finished product was given the designation IL-TiO_2-NPs.

2.5. Preparation of IL-TiO_2-NPs@MWCNTs@GO/GCE

Before use, the GCE was polished with an alumina slurry to obtain a mirror-like surface, then washed with deionized water and sonicated with ethanol and deionized water (50:50) to remove alumina particles from the electrode surface. It was finally rinsed with deionized water and dried in an oven. 0.20 mg of MWCNT was dissolved in 10 mL of N, N-dimethyl formamide (DMF) and then kept in ultra-sonication for 60 min, which finally resulted in a black suspension, which was used for GCE modification. Then, 0.30 mg of IL-TiO_2 and 0.30 mg of MWCNT were dispersed in 30 mL of DMF by ultra-sonication for 2 h to give a black suspension. The resulting dispersion (5 µL -IL-TiO_2-NPs@MWCNTs@GO/GCE) was deposited on the surface of the GCE and held for drying in an oven at 60°C for about 10 min.

The electrode was then cooled to room temperature, resulting in the product IL-TiO_2-NPs@MWCNTs@GO/GCE.

2.6. Real Sample Preparation

Samples of tablets containing the antibiotic Azithromycin were purchased from a local pharmacy. The presence of the antibiotic Azithromycin in the marketed tablets was tested using the following procedure. 10 tablets were weighed and crushed to obtain a fine powder sample. A 5 mg sample of tablets was then transferred to a 100 mL volumetric flask and dissolved in PBS. The resulting mixture was sonicated for 20 minutes. Analyses were performed by the standard addition method using the DPV technique and the cpator made IL-TiO_2-NPs@MWCNTs/GCE.

For the preparation of biological samples such as human urine or serum, 5 mL of sample (from healthy volunteers) was transferred to a 100 ml volumetric flask, and diluted with 0.1 M H_2SO_4. The samples, human urine or blood serum, were transferred to our laboratory centrifuge and centrifuged at a speed of 1000 rpm for 30 minutes. Voltammograms were obtained, showing the absence of observed peaks associated with the electro-oxidation of the antibiotic Azithromycin molecules after this test. Then, 5 mL of the filtered solution, along with different amounts of Azithromycin concentrations (these concentrations were 10^{-5} M, 510^{-6} M and 10^{-6} M), were directed to the electrochemical cell and the corresponding voltammograms were recorded with IL-TiO_2-NPs@MWCNTs/GCE. Thus, the concentration of Azithromycin antibiotic molecules in each solution was measured using the standard addition procedure

3. RESULTS AND DISCUSSION

3.1. Characterization of IL-TiO_2 NPs@MWCNTs/GO/GCE by scanning electron microscope

Figure 1 shows the scanning electron microscope images of the surface morphology of the IL-TiO_2 NPs@MWCNTs/GO/GCE electrode and the unmodified MWCNTs/GO/GCE electrode. From the examination of these images, the surface of the modified paste was completely covered with TiO_2 nanoparticles of extremely varied sizes at a magnification of 2 µm over the entire surface of the paste prepared for our fabricated sensors. It is well observed that the GO exhibits two-dimensional sheet-like layers with typical wrinkles (Figure 1A) compared to the irregularly aggregated TiO_2 nanoparticles on the graphene oxide sheets [44]. The as-prepared TiO_2 NPs@MWCNTs/GO Composites The as-prepared TiO_2 NPs@MWCNTs/GOs reveal the structures of the titanium oxides attached from the benzene ring to the carbon ring of the graphene via a π-π interaction. From the image of the as-synthesized TiO_2-MWCNTs/GO composites, a large number of TiO_2 nanoparticles cover the surface of the GO nanosheet (Figure 1B and C) [52]. These results increase the chances of

recognition of antimicrobial azithromycin molecules by the receptor part of IL-TiO_2 NPs@MWCNTs/GO/GCE electrode and lead to the oxidation of the active center of azithromycin molecules.

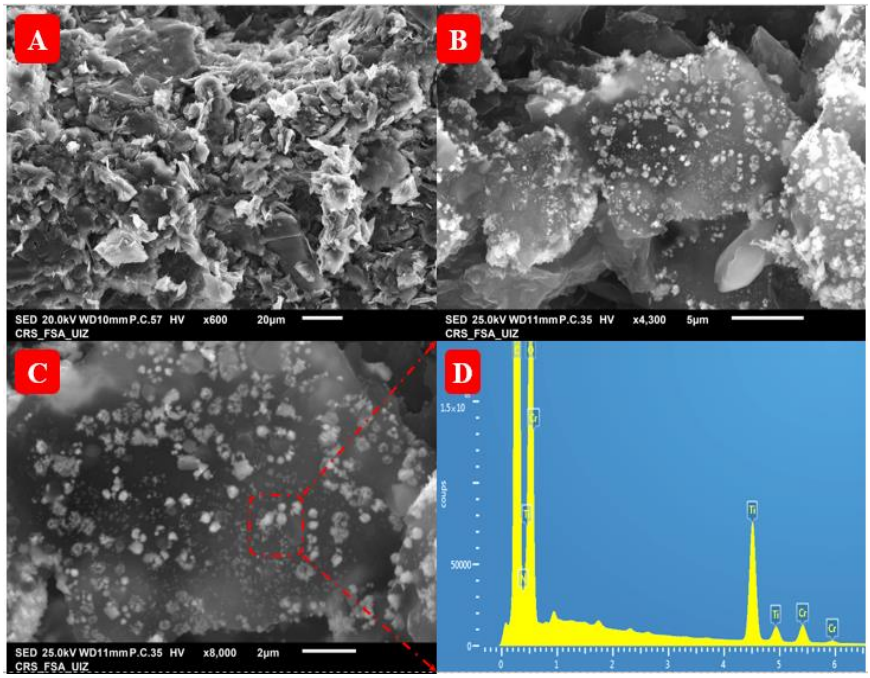

Figure 1. SEM scan: (A) of unmodified MWCNTs/GO/ GCE; (B) and (C) of IL-TiO_2 NPs@MWCNTs/GO/GCE at different positions and (D) by EDX

The elemental chemical composition of our IL-TiO_2 NPs@MWCNTs/GO/GCE electrode composite was analyzed by EDX (energy dispersive X-ray analysis). The analysis spectrum Figure 1D shows the presence of five peaks with the characteristics of the element titanium, and carbon one peak that characterizes the element oxygen and the atomic percentage of O is about twice that of Ti. This raises that TiO_2 was prepared and successfully applied on the surface of Multiwall carbon nanotubes-graphene oxide (MWCNTs/GO). Therefore, the presence and distribution of TiO_2 nanoparticles enhanced the electron transfer kinetics between the surface and the target electroactive species and also created conductive electron bridges to the electroactive species located near the surface of the working electrodes.

3.2. Characterization of IL-TiO_2 NPs@MWCNTs/GO/GCE by X‑ray diffraction

By using the X-ray diffraction technique, the structural characterization of the IL-TiO_2 NPs@MWCNTs/GO/GCE sensor composites was performed out. Figure 2 displays the X-ray diffraction spectra of the anatase sensor composites produced through aided processing at (T=80°C, TH=1H) temperatures. The acquired spectra show that there are multiple peaks present. The initial planes of these peaks (no impurity peaks) are (101), (004), (200), (105), (211), (204), (116), (220), and (215), and they correspond to the anatase phase at 2θ =25.3°;

37.9°; 48.1°; 54.0°; 55.2°; 62.8°; 68.9°; 70.4° and 75.2°, respectively [53]. The PXRD models of the rutile and anatase phases are attributed to the peaks of the TiO_2 NPs (JCPDS 73-1764 & JCPDS 78-1510). The first peak, which corresponds to the (101) plane at 2θ=25° [54], the strongest, is. The fact that this peak exists and the peak at 27.45°, which is indicative of the rutile phase, does not indicate that the annealing procedure was ineffective in producing the anatase phase. It is noted that the TiO_2 -NPs nanocomposite formed on graphite carbon oxide sheets using the procedure used and described in section 2.3 have improved crystallinity. The obtained nanocomposites XRD patterns reveal a highly crystalline TiO_2 structure, no precursor- or reactant-related impurity peaks, and the absence of GO diffraction peaks in the composite made of TiO_2/MWCNTs/GO, which shows that GO has been effectively reduced and that there is stacking between the graphene sheets. These structural characterizations help confirm the successful immobilization of TiO_2 on GO by the hydrothermal procedure[52,55] . Additionally, this XRD result demonstrates that NPs -TiO_2 have a sizable active surface area that ensures closer proximity to the electroactive components of the antibiotic azithromycin as well as a potent electro-catalytic effect that facilitates the conversion of the NO_2 attraction groups in the side chain of the antibiotic azithromycin into NHOH groups into a quantifiable and understandable electrical signal. This conclusion of the nano TiO_2 –NPs @MWCNTs/GO composites XRD patterns is substantially consistent with the work performed out by our team, Zoubir Jallal et All.

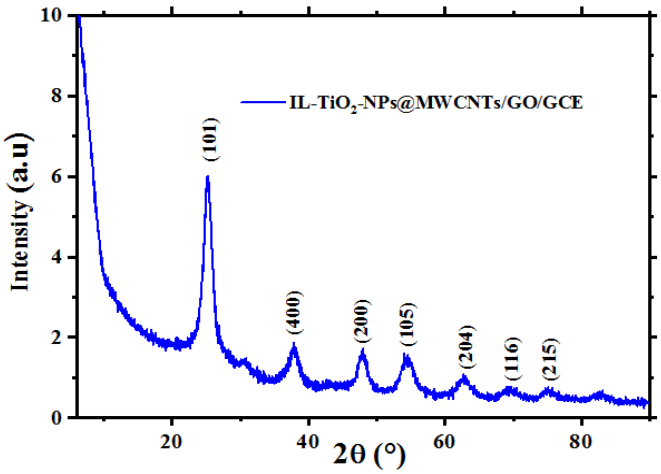

Figure 2. X-ray diffraction (XRD) of IL-TiO_2 NPs@MWCNTs/GO/GCE constructed

3.3. Characterization of TiO_2-NPs@MWCNTs@GO/GCE and MWCNTs/GO by Infrared Spectroscopy

Figure 3 shows the FTIR spectra of GO and TiO_2 -NPs@MWCNTs/GO. Numerous peaks corresponding to oxygen-containing functional groups are seen in these spectra, including the stretching vibration of the -OH group (3388 and 1623 cm^{-1}), C=O of C=O-O-H groups (1725

cm-1), C-O of C=O-O-H groups (1069 cm^{-1}), and C-O-H (1382 cm Around 1558 and 1189 cm^{-1}, two additional peaks that are related to the graphite sheets C=C skeletal vibration can be seen [56,57]. A clearly broad peak at at 3206 cm^{-1} and a sharp peak at 1622 cm^{-1} are seen in the spectra of TiO_2 and TiO_2 -NPs @@MWCNTs/GO composites, which are attributed to the O-H stretching vibration and C=C skeletal vibration of the graphite sheet, respectively. The peak at around 509 cm^{-1}, attributable to the Ti-O-Ti stretching vibration, reveals the synthesis of nanoparticles resembling TiO_2 and encourages the development of metallic oxygen bonds in titanium. Consequently, this catalytic activity of the surface of our electrodes created against the active center of the AZT molecules can be justified by the TiO_2 phase dispersed and distributed over the graphene oxide sheets alone.

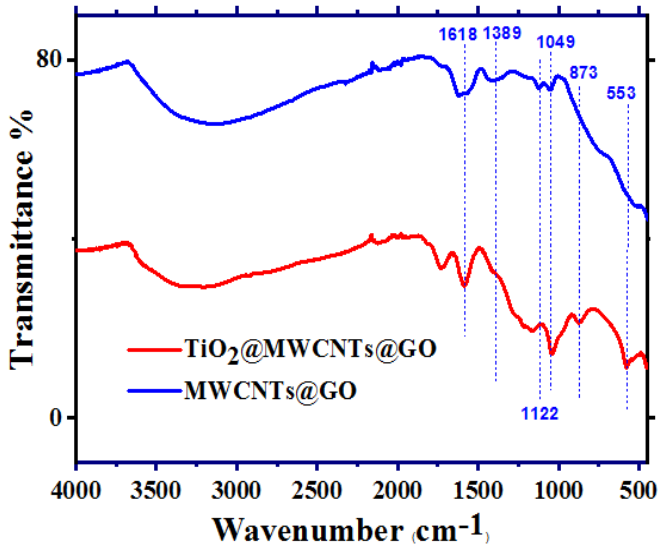

Figure 3. Infrared Spectroscopy of IL-TiO_2 NPs@MWCNTs/GO/GCE constructed and Unmodified of MWCNTs/GO/GCE

3.4. Characterization of IL-TiO_2 NPs@MWCNTs/GO/GCE by Raman spectroscopy

Figure 4 displays the Raman spectroscopy results for the recording of TiO_2 NPs@MWCNTs/GO/GCE. In the data, the anatase phase of TiO_2 is revealed by typical peaks of TiO2 NPs centered at 146 (Eg), 180 (Eg), 397 (B1g), 514 (A1g), and 637 cm^{-1} (Eg), as well as by a weaker peak at 445 cm^{-1} (Eg), which may be related to the rutile phase. Peak intensities show that pure TiO_2 NPs had a higher percentage of the anatase phase than the rutile phase, which had a greater electrocatalytic impact on the active sites of azithromycin molecules[53]. We also have two peaks located at the positions of 1350 cm^{-1} and 1650 cm^{-1} that characterize the Raman spectrum of GO: a G-band at about 1600 cm^{-1} and a D-band at about 1350 cm^{-1}, corresponding to the E_2g phonon of C sp^2 atoms and a k-point phonon respiration mode of A_1g symmetry, respectively [58,59].

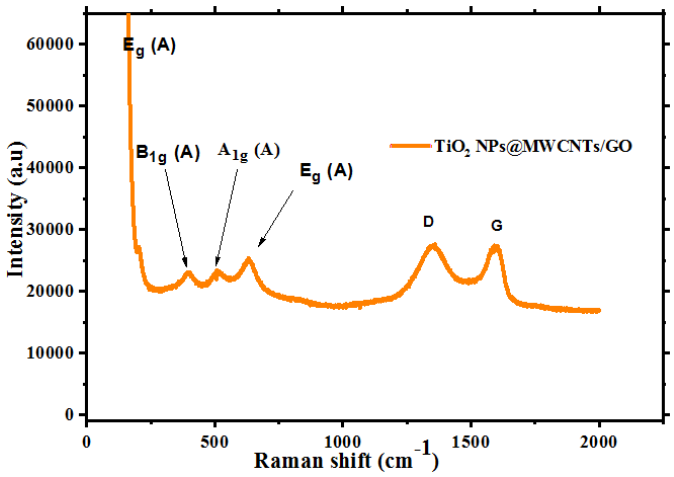

Figure 4. Raman spectra of IL-TiO_2 -NPs@MWCNTs/GO/GCE

3.5. Comparison between IL-TiO_2 NPs@MWCNTs/GO/GCE and MWCNTs/GO/GCE by using cyclic voltammetry

In this part, the surface of unmodified GO/GCE, MWCNTs/GCE, MWCNTs/GO/GCE, and IL-TiO_2 NPs@MWCNTs/GO/GCE electrodes made by CV and EIS were probed using the electrochemical redox behavior of $Fe(CN)_6^{3-/4-}$. Figure 5 displays the CV of a $Fe(CN)_6^{3-/4-}$ KCl solution on the electrode surface of IL-TiO_2 NPs@MWCNTs/GO/GCE, GO/GCE, MWCNTs/GCE, and MWCNTs/GO/GCE, respectively, at a potential of 20 $mv.s^{-1}$. Due to the poor permeability of multiwall carbon nanotubes brought on by the absence of recognition cavities and the limitation of nonspecific currents, there was no high intensity redox probe current peak at MWCNTs/GCE multiwall carbon nanotubes, as demonstrated in the curve in Figure 5.

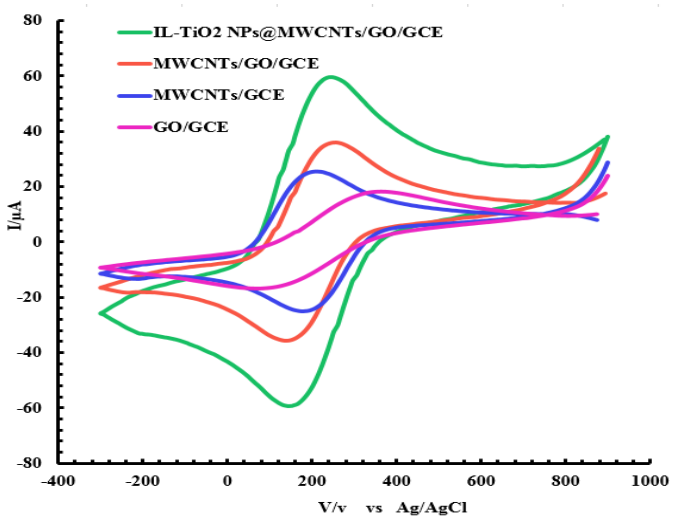

Figure 5. Cyclic voltammograms of Graphene nu modified, IL-TiO_2 NPs@MWCNTs/GO/ GCE; MWCNTs/GO/GCE; MWCNTs/ GCE and GO /GCE. Results obtained in a solution of 1 mM $Fe(CN)_6^{¾-}$ and 0.5 M KCl at a scan rate of 20 mV s^{-1}

The best response was observed on the interface of the IL-TiO_2 NPs@MWCNTs/ GO/GCE sensor, according to the results shown in Figure 5 indicating good communication between the sensor and the active centers of $Fe(CN)_6^{3-/4-}$ molecules. Therefore, the IL-TiO_2 NPs@MWCNTs/GO/GCE sensor shows a very high active center recognition performance compared to other electrodes [52].

Figure 5 illustrates the reversible CV that the $Fe(CN)_6^{3-/4-}$ showed on the IL-TiO_2-NPs@MWCNTs/GO/GCE after the IL-NPs-TiO_2 were added to the MWCNTs. The cavities in the IL-NPs-TiO_2 allow the probe to transfer to the electrode surface, which significantly improves the electron transfer between the $Fe(CN)_6^{3-/4-}$ and electrode surface. This result is a reflection of the extremely high electronic conductivity of the working electrode surface modified with IL-TiO_2 NPs@MWCNTs/GO/GCE, which results in an extremely quick electron transfer. We have molecules of the $Fe(CN)_6^{3-/4-}$ in the IL-TiO_2-NPs@MWCNTs/GO/GCE-supported electrolyte, and the presence of IL-NPs-TiO_2 on the combination of multiwall carbon nanotubes and graphene oxide sheets creates highly conductive bridges that amplify the electrostatic attraction at the interface.

3.6. Comparison between IL-TiO_2 -NPs@MWCNTs/GO/GCE and MWCNTs/GO/GCE by using impedance spectroscopy

EIS was also used to characterize the different modified electrodes. As shown in Figure 6, the R_{ct} values of the different electrodes were classified as follows: R_{ct} (IL-TiO_2 NPs@MWCNTs/GO/GCE) < R_{ct} (MWCNTs/GCE). This decrease in Rct was in agreement with that of the CV measurements as shown in Figure 6.

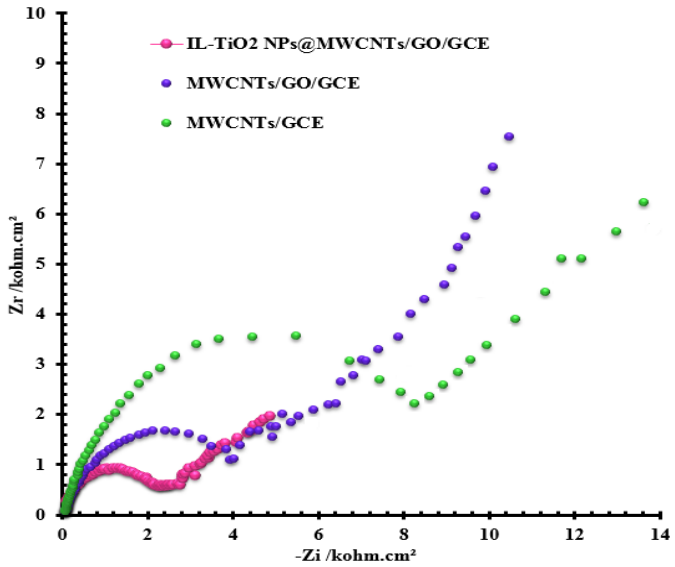

Figure 6. EIS obtained in a ferric/ferrous solution (1 mM ferric/ferrous and 0.1 M KCl) in the frequency range from 0.1 Hz to 100 kHz at 0.25 V *vs.* Ag/AgCl by applying a potential (AC) of 10 mV

The analysis of these curves demonstrates that a semicircle with a diameter equal to the charge transfer resistance R_{ct} (MWCNTs/GO/GCE)=4.2 kOhm/cm^2, which controls the electron transfer kinetics of the $Fe(CN)_6^{3-/4-}$ at the interface of the unmodified MWCNTs/GO/GCE electrode, is present on the bare MWCNTs/GCE electrode in the high frequency range. This means that the electrostatic attraction at However, following its modification by IL-NPs-TiO_2, we see a little semicircle in the high frequency region with a very small diameter, indicating a significant reduction in the charge transfer resistance, as indicated by R_{ct} (IL-TiO_2 NPs@MWCNTs/GO/GCE) =2.21 kOhm/cm^2. Showing a significant electrostatic attraction between the changed interface and the negatively charged molecules of the $Fe(CN)_6^{3-/4-}$ system due to the fast electron transfer kinetics. These results suggest that the IL-TiO_2 NPs@MWCNTs/GO/GCE sensor had a significant impact on both the increase of electron transfer between the redox centers and the surface of the constructed electrode as well as the identification of the model molecule of Azithromycin.

3.7. Electrochemical behaviors of Azithromycine

3.7.1. Optimization of the MWNT preparation amount

To increase the number of active sites for the identification of the antibiotic Azithromycin molecules and hence increase the effectiveness of the treatment, multi-walled carbon nanotubes (MWNTs) were incorporated into the GCE cavity. Based on the extensive surface area and high conductivity of the multiwall carbon nanotubes, the goal was to increase the number of active sites for the recognition of azithromycin antibiotic molecules and thereby increase the oxidation response current of azithromycin antibiotic molecules on the interface of IL-TiO_2 NPs@MWCNTs/GO/GCE sensor (MWNTs).

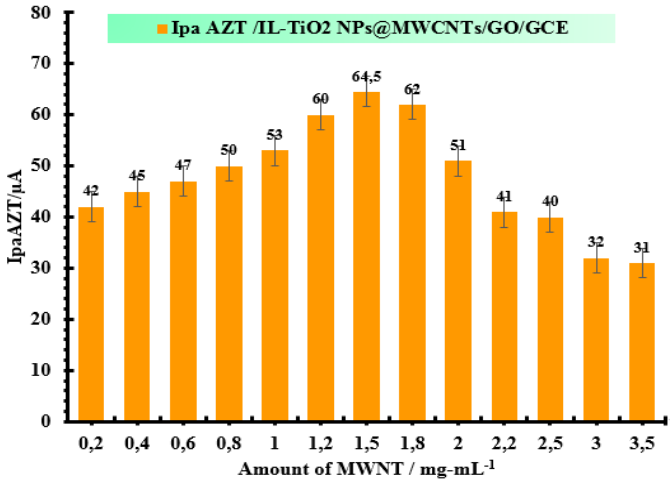

Figure 7. Responses CVs of electrooxidation of Azithromycin on electrode IL-TiO_2-NPs@MWCNTs/GO/GCE in PBS (pH = 7) at a scan rate of 20 mV/s

Also, the interaction between the antibiotic Azithromycin and the MWNTs nanocomposites may enhance the sensitivity and selectivity of the electrocatalytic reaction occurring at the sensor interface. Figure 7 shows the optimal amount of multi-walled carbon nanotubes needed to create IL-TiO_2@MWCNTs/ GO/GCE NPs. In the range of 0.2 to 3.50 mg.mL^{-1}, the ideal MWNT concentration for the fabrication of IL-TiO_2 -NPs@MWCNTs/GO/GCE was examined. The MWNTs functioned as a functional monomer in the precursor solution for the IL-TiO_2-NPs@MWCNTs/GO/GCE sensor, which was advantageous for the development of more active sites for the recognition of the active center of the side chain of the target molecules of the antibiotic azithromycin.

The results in Figure 7 show that the number of multi-walled carbon nanotubes combined with IL-TiO_2 NPs and graphene oxide increases the intensity of the oxidation peak of Azithromycin antibiotic molecules, suggesting that the multi-walled carbon nanotubes improve the sensitivity of the electrode. Nevertheless, the current intensity decreases once 1.50 mg. mL^{-1} of multiwall carbon nanotubes are present. In fact, too many multiwall carbon nanotubes produce a lot of background current and noise, which makes it difficult to identify the antibiotic Azithromycin molecules.

Therefore, a reasonable amount of 1.50 mg.mL^{-1} multiwall carbon nanotubes played a very important role in the recognition of the model molecule and the enhancement of electron transfer between the redox centers and the electrode surface was chosen for the fabrication of IL-TiO_2 NPs@MWCNTs/GO/GCE in order to create more efficient recognition cavities and achieve a fast response.

3.7.2. Study of electrochemical behavior of Azithromycin at IL-TiO_2 NPs@MWCNTs/ GO/GCE

Azithromycin antibiotic molecules (0.1 mM) were electrooxidized using a cyclic voltammetry approach on the composite electrode of a modified IL-TiO_2-NPs@MWCNTs/GO/GCE sensor in a pH 7.0 PBS electrolyte solution. Due to the large conductive surface area, it was found that there is a significant improvement in the electrooxidation behavior of Azithromycin antibiotic molecules on the sensor interface of the modified IL-TiO_2 NPs@MWCNTs/GO/GCE compared to MWCNTs/GO/GCE and MWCNTs/GCE. electrode. This proves that the modification of MWCNTs/GO/GCE is effective.

The excellent properties of IL-TiO_2 NPs nanoparticles with ionic liquid, such as catalytic property, large surface area, high electrical conductivity and fast electron transmission, as well as excellent electro-catalytic activity, are clearly apparent in the voltammetry results, which clearly show an increase in the peak current of electro-oxidation of azithromycin molecules on the constructed electrode. On the modified IL-TiO_2 NPs@MWCNTs/GO/GCE sensor, the peak current of electro-oxidation of azithromycin antibiotic molecules was reported to be 50.92 µA, and on the unmodified MWCNTs/GO/GCE sensor, the peak current is 22.42 µA, as shown

in Figure 8. The peak potential of electrooxidation of azithromycin antibiotic molecules at the fabricated electrode is 0.512 V (*vs.* Ag/AgCl), while the peak potential at the unmodified MWCNTs/GO/GCE electrode is 0.48 V (*vs.* Ag/AgCl). The electrochemical behavior of azithromycin antibiotic molecules in this research study is reversible.

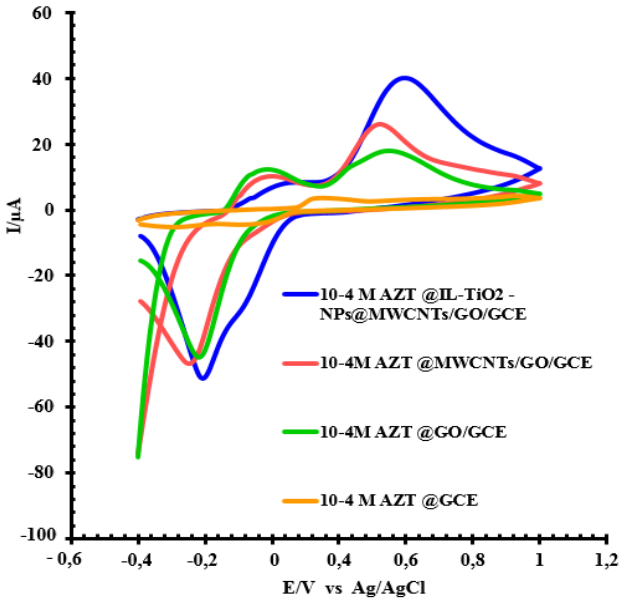

Figure 8. CVs responses of electrooxidation of Azithromycin molecules on IL-TiO_2@MWCNTs/GO/GCE and MWCNTs@GO/GCE; GO/GCE; unmodified GCE bar in PBS (pH = 7) at a scan rate of 20 mV/s

3.7.3. Study of sweep rate variation

We examined the effect of scan rates ranging from 20 to 200 mV/s of 10^{-3} M Azithromycin antibiotic molecules in 0.1 M phosphate buffers at (pH=7) in order to better understand the electrochemical mechanism of electro-oxidation of Azithromycin antibiotic molecules on the electro-catalytic surface of the proposed modified IL-TiO_2 NPs@MWCNTs/GO/GCE electrode between 0 and 1200 mV/Ag/AgCl on the cyclic voltmeter (Figure 9A).

Sensor IL-TiO_2 NPs@MWCNTs/GO/GCE was treated to a CV measurement to examine the impact of scan rate (Figure 9A). Peak current increased linearly and scan rate gradually increased with an increase in scan rate from 20 to 200 $mV.s^{-1}$. Indicating a surface-controlled, diffusion-free process of IL-TiO_2 NPs@MWCNTs/GO/GCE during the oxidation of azithromycin antibiotic molecules, the peak current increased linearly along with a gradual shift of the peak potential of the oxidation of Azithromycin antibiotic molecules in the positive direction. Figure 9B represents the linear regression equation for the anodic I_{pa} and cathodic I_{pc} peaks via scan rate. I_{pc} (AZT/µA) = -0.01707 v ($mV.s^{-1}$) -27.326 (R2=0.98580) and I_{pa} (AZT/µA) = 0.0201 v ($mV.s^{-1}$) +25.613 (R^2=0.9761), respectively. Additionally, we used the root of the scanning speed shown in Figure 9C. to display the intensity curves of the anodic I_{pa}

and cathodic I_{pc} peaks: The linear regression equation is represented by I_{pc} (AZT/µA) = -5.0154 $v^{1/2}$ (mV.s^{-1}) -10.645 (R^2=0.980) and Ipa (AZT/µA) = 5.6501 $v^{1/2}$ (mV.s^{-1}) +7.8951 (R^2=0.977).

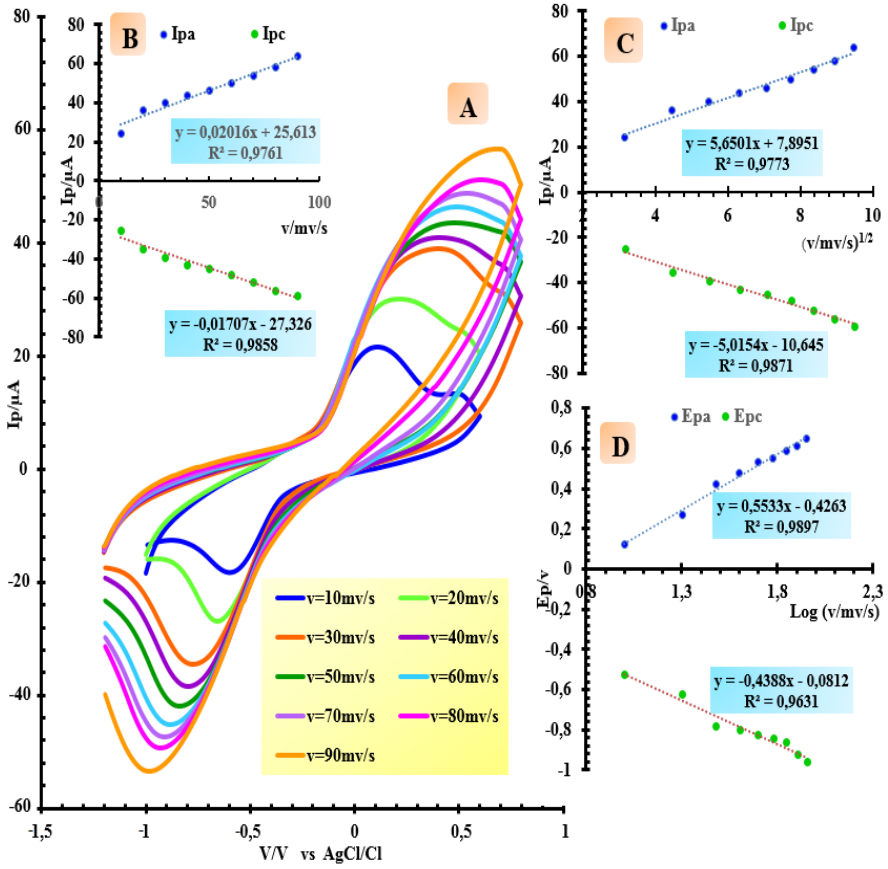

Figure 9. CVs response of electrode constructed of 1 mM of Azithromycine with different scan rates (20-120 mV/s) at pH =7 (A). Curve of I_{pa} and I_{pc} versus v(mV/s) (B) and plot of I_{pa} and I_{pc} versus $v^{1/2}$/(mV/s)$^{1/2}$ (C). Variation of E_{pa} and E_{pc} as a function of Log (v/ mV/s) (D)

These findings enable us to suggest that diffusion processes within the measurement cell employed govern the evolution of the active surface of the IL-TiO_2 NPs@MWCNTs/GO/GCE electrode during the oxidation reaction of the Azithromycin antibiotic molecules. This phenomenon and what J.Y. Peng and All [17] discovered in their investigation are remarkably comparable. It illustrates both the ideal situation for quantitative detections of the antibiotic azithromycin in actual samples and the ideal setting for the creation of a quick and effective detection tool for these molecules.

Figure 9D shows the relationship between the Azithromycin antibiotic molecules' oxidation peak potential and the scan rate's logarithm (v). The peak potential values vary linearly with the logarithm of the scanning speed Log (v), as shown in Figure 9.D, with regression equations E_{pa} (AZT) =-0. 5533Log (v/mV.s^{-1}) - 0.4263 and E_{pc} (AZT) = -0. 4388Log (v/mV.s^{-1}) - 0.0812 with correlation coefficients (R^2 = 0.9897) and (R^2 = 0.9631) in the range of 10 As a result, the peak potentials are very sensitive to the speed of electron transmission throughout the scan.

Laviron showed that the equation between E_{pc} and Log (v) (Eq. 1 and Eq. 2) is true when a system is reversible [17,60].

$$E_{pa}(\mathrm{AZT}) = \mathrm{E°} - \frac{\mathrm{RT}}{(1-\alpha)\mathrm{nF}}\mathrm{Ln}\,\frac{(1-\alpha)\mathrm{nF}}{\mathrm{kRT}} - \frac{\mathrm{RT}}{(1-\alpha)\mathrm{nF}}\,\mathrm{LnV} \qquad (\mathrm{Eq.}\,1)$$

$$\mathrm{Spa} = \frac{\mathrm{RT}}{(1-\alpha)\mathrm{nF}}$$

$$E_{pc}(\mathrm{AZT}) = \mathrm{E°} - \frac{\mathrm{RT}}{\alpha\mathrm{nF}}\mathrm{Ln}\,\frac{\alpha\mathrm{nF}}{\mathrm{kRT}} - \frac{\mathrm{RT}}{\alpha\mathrm{nF}}\,\mathrm{LnV} \quad (\mathrm{Eq.}\,2)$$

$$\mathrm{Spc} = -\frac{\mathrm{RT}}{\alpha\mathrm{nF}}$$

The perfect gas constant is R. (8.31SI). The electron transfer coefficient is written as. The outside temperature is T. (298k). The battery constant is F. (96546C). The peak potential vs. Ag/AgCl of our constructed sensor is the peak potential of the number of electrons that azithromycin antibiotic molecules have captured for the reduction step on the electro-catalytic surface. The Spa/Spc ratio=α/(1-α)=1.2609 to determine the value of the transfer coefficient α was estimated to be 0.5576. In effect, we find a value equal to 1.2609 after taking into account the slope of the equation obtained by linearizing Epc as a function of Log (v) and the slope of the Laviron Equation 1 and 2. For a fully reversible system, α is often estimated to be a value of 0.5576 Therefore, 1.88 (n=2) electrons were transported to the surface of the modified electrode during the reaction of the antibacterial molecule azithromycin.

3.7.4. Study of Effect of an accumulation time

By oxidizing or diminishing the analytes present on the electrode surface, the coexistence of analytes can have a considerable impact on the electrochemical response. As shown in Figure 10, the peak current of the curve was maximum at 120 seconds after the effect of accumulation was done on the surface of IL-TiO_2-NPs@MWCNTs/GCE in the range of 0-400 s while antibiotic molecules of azithromycin were present. As a result, additional research was done without any accumulating time.

We investigate that the current intensity of the reduction peak of azithromycin antibiotic molecules increases nearly linearly with accumulation time up to a time point equal to 120s without electrode surface saturation, demonstrating that the IL-TiO_2-NPs@MWCNTs@GO/GCE has a substantial active surface area as well as good analytical performance. This time period is interesting. We also notice, after 120s, a stabilization of the peak current intensity of the electro-oxidation of azithromycin antibiotic molecules, which indicates that the surface has been saturated, lowering the electrode's performance. This investigation determined that a period of 120 s was the best accumulation time for achieving excellent sensitivity and a manageable analysis time.

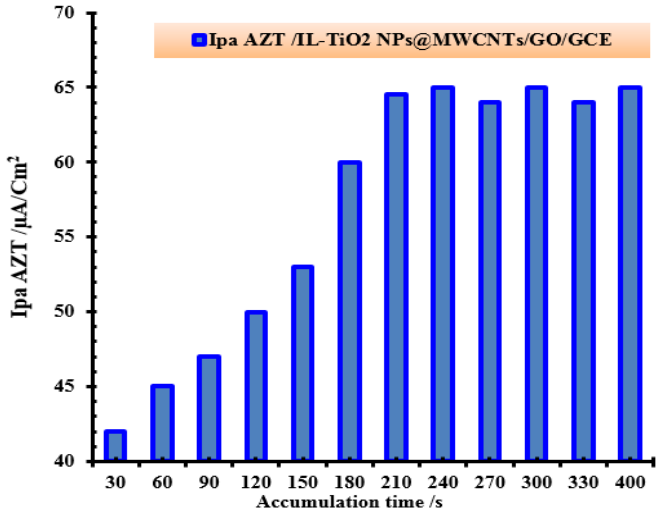

Figure 10. The effect of accumulation time of 10^{-4} M electrooxidation of Azithromycin on the IL-TiO_2-NPs@MWCNTs@GO/GCE sensor at a scan rate of 20 mV/s

3.7.5. Study of effect of pH

The effect of pH on the response of azithromycin antibacterial molecule current was investigated by CV on the sensor IL-TiO_2 NPs@MWCNTs/GO/GCE face in a tampon phosphate 0,1M solution with varying pH values (pH 3.0 to pH 9.0) at a balayage speed of 20 mVs^{-1}. As shown in Figure 11, we can see that the intensity of the point current of electro-oxidation increases with pH, and the maximum current of the antibacterial drug azithromycin molecules was activated at pH 7.0. In order to fully understand all of these phenomena, the same tampon phosphate solution (pH 7.0) was chosen to explore further phenomena that arise at the interface of the IL-TiO_2 NPs@MWCNTs/GO/GCE.

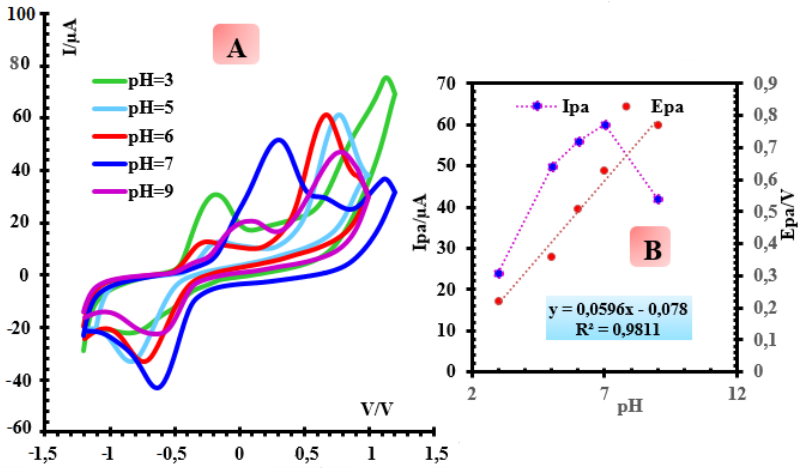

Figure 11. (A) Cyclic voltammograms (at 20 mV/s) of 1.0×10^{-4} M electrooxidation of Azithromycin on IL-TiO_2 NPs@MWCNTs/GO/GCE constructed at different values of (pH= 3 to 9); Inset: (B) Plot of E_{pa} versus pH and I_{pa} versus pH

In Figure 11, the voltammograms were presented. The change of potentials to lower positive values with increasing pH was used to highlight the role of protons in the electro-oxidation of the antibiotic Azithromycin molecules. Following was determined to be the linear regression equation for the plot of E_{pa} versus pH: Indicating that the number of electrons transferred during the electrooxidation process of the azithromycin antibiotic molecules was equal to the number of protons transferred, the slope of the regression equation was discovered to be similar to the theoretical value of 0.059 V pH^{-1} (298 K) [17,20]. The surface of the IL-TiO_2 NPs@MWCNTs/GO/GCE sensor interacts more readily with the active sites of azithromycin antibiotic molecules when the medium is at pH 7, as a result.

The schematic most probably depicts how the oxidation of azithromycin at the interface of the IL-TiO_2-NPs@MWCNTs/GO/GCE sensor proceeds Scheme 1.

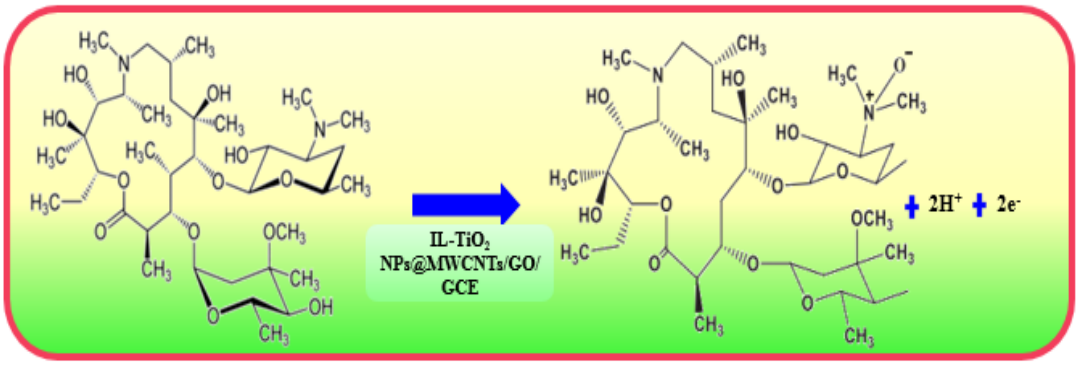

Scheme 1. Electrochemistry of azithromycin electrooxidation at the IL-TiO_2 NPs@MWCNTs/GO/GCE sensor interface in phosphate buffer (PBS) (pH =7)

3.8. Analytical applications

3.8.1. Detection limit and calibration curve

The manufactured IL-TiO_2-NPs@MWCNTs/GO/GCE sensor carried out a calibration to evaluate the analytical performance of the established method for the detection of electro-oxidation of azithromycin antibiotic molecules. The experiment was carried out under ideal measuring circumstances (a pH 7.0 supporting electrolyte (PBS) and a 20 mV/s scan rate). Figure 12A displays the relationship between the concentration of azithromycin antibiotic molecules in the electrochemical cell and their electrooxidation current peak as well as the associated voltammograms Figure 12 displays an electrochemical cell and the accompanying voltammograms. As can be shown, by adjusting the Azithromycin concentrations at the IL-TiO_2 NPs@MWCNTs/GO/GCE sensor from 10^{-3} M to 10^{-7} M, great linearity, strong sensitivity, and lowest background current were obtained (Figure 12A). Two linear ranges were found: 10^{-3} to 10^{-6} M with equation $I_{pa\ (AZT)} = 0.6678[AZT] + 46.588$ with a coefficient (R^2= 0.9933) and 10^{-6} to 10^{-7} M with equation $I_{pa\ (AZT)} = 10.876[AZT] + 15.455$ with a coefficient (R^2= 0.7178). The computed LOD and LOQ values, which were equivalent to 1.772×10^{-8} M

and 5.83×10^{-8} M respectively, were based on the data acquired (LOQ = 3 s/b; LOQ = 10 s/b, where s-signal noise, b-slope of calibration). Table 1 compares the analytical performance of IL-TiO_2 NPs@MWCNTs/GO/GCE with other modified electrodes for the detection of azithromycin molecules that have been reported in the literature. The constructed IL-TiO_2 NPs@MWCNTs/GO/GCE sensors usefulness as well as the proposed method's effectiveness were examined.

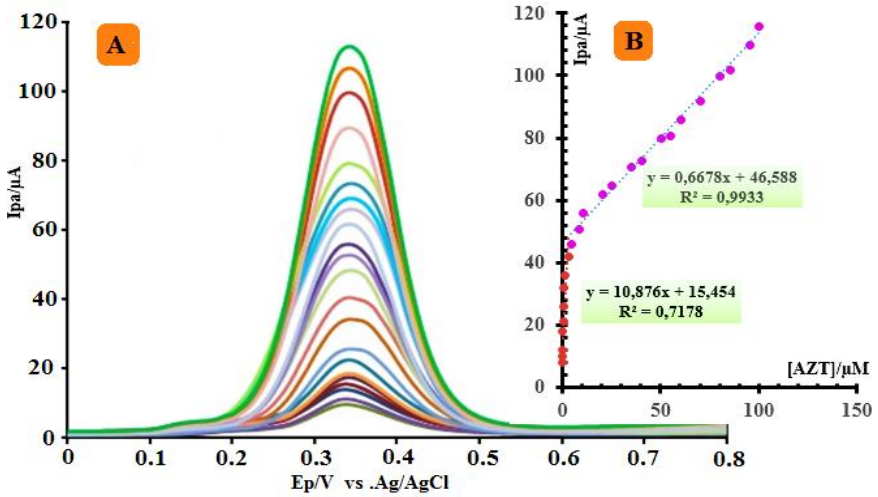

Figure 12. DPV of Azithromycine in 0.1 M phosphate buffer (pH=7) for {100 ;80 ;70 ;60 ;50; 40; 30; 20; 15; 10; 8; 6; 4; 2; 1; 0.8 µM}(A), Inset: plots of electrocatalytic peak current versus Azithromycine concentration (B)

Table 1. Comparison of the performance of our IL-TiO_2 NPs@MWCNTs/GO/GCE sensors with different sensors from the literature

Electrode materials	Detection Method	Electrolyte	Linear dynamic range (µM)	LOD (µM)	Ref.
MIP/ABP electrode	**DPV**	**PBS**	**100.0–2000**	**0.0111**	**[61]**
GR/IL/GCE	**DPV**	**PBS**	**650.0–3800 nM**	**0.25**	**[17]**
$MgCr_2O_4$-MWCNT/GCE	**DPV**	**PBS**	**250–10,000**	**0.07**	**[20]**
GO/MWCNT/GCE	**DPV**	**PBS**	**100–1000**	**0.07**	**[41]**
MIP Bth/3-TBA	**DPV**	**PBS**	**13.33 –66.66**	**0.85**	**[11]**
MIP/GNU/GO/GCE	**DPV**	**PBS**	**0.3–920**	**0.1**	**[24]**
MIP-PVC membrane	**DPV**	**PBS**	**0.6–10000**	**0.5**	**[62]**
IL-TiO_2 NPs@MWCNTs/GO/GCE	**DPV**	**PBS**	**0.1-1000**	**1.772×10^{-2}**	**This work**

It was established how much of the antibiotic azithromycin was present in the real samples. The procedures outlined in section 2.3 were followed in order to manufacture the pharmaceutical goods in tablet form and the samples (human blood, urine), which were then quantified using the conventional addition method. In section 2.6, the technique is described.The results are displayed in Table 2. Recovery rates computed using samples assessed by the IL-TiO_2 NPs@MWCNTs/GO/GCE sensor ranged from 97 to 99.3%, indicating that the approach created for identifying azithromycin antibiotic molecules by the IL-TiO_2 NPs@MWCNTs/GO/GCE sensor can be regarded as accurate.

3.8.2. Repeatability, reproducibility and stability

The developed IL-TiO_2 NPs@MWCNTs/GO/GCE electrodes repeatability was assessed by performing five consecutive tests to detect 10^{-4} M molecules of the antibiotic azithromycin. The measurements' relative standard deviation (RSD) was calculated to be 4.42%. By constructing five electrodes in the same way, the reproducibility of the measurements of the built-in IL-TiO_2 NPs@MWCNTs/GO/GCE electrode was also examined. Using the same experimental conditions as before, these were then used to identify antibiotic molecules with a molecular weight of 10^{-4} M. For the five electrodes under study, the relative standard deviation was calculated to be 3.23%. We additionally test the IL-TiO_2 NPs@MWCNTs/GO/GCE sensors storage stability by detecting 10^{-4}M azithromycin over 25 days at 20°C; the electrode maintained 96% of its initial response, proving the viability of the sensor tissue. These statistical findings therefore show that the IL-TiO_2 NPs@MWCNTs/GO/GCE electrode exhibits very excellent repeatability, reproducibility, and stability.

3.8.3. Response of IL-TiO_2 NPs@MWCNTs/GO/GCE sensor in the presence of interferents

The detection of the quantities of the antibiotic Azithromycin antibiotic molecules may be hampered by the presence of specific anti-target compounds in the tested samples (human blood, urine). Because of this, it is important to assess the selectivity of the IL-TiO_2 NPs@MWCNTs/GO/GCE electrode designed for the detection of azithromycin antibiotic molecules in a complex matrix and to spot any potential issues caused by the presence of these interfering components. We looked at how different compounds affected the ability to detect 10^{-5} M of the antibiotic azithromycin after adding 10-fold excesses of Cl^-, K^+, NO^{3-}, HCO_3^-, CO_3^-, Ni^{2+}, Cu^{2+}, Zn^{2+}, Pb^{2+}, Mg^{2+}, Ca^{2+}, Al^{3+}, SO_4^{2-} and Fe^{3+}. By using cyclic voltammetry in the potential range of 0 mV to 1100 mV with a sweep rate of 20 mV/s and the presence of 10-fold concentrations of biological species including starch, glucose, urea, uric acid, and ascorbic acid. Only uric acid showed an anodic peak at +0.35 V, but azithromycin antibiotic molecules only saw a 3.9% rise in peak current. This shows that the suggested sensor can be utilized to identify the antibiotic azithromycin in samples with confidence. The recovery rate for the current intensity recorded on the IL-TiO_2 NPs@MWCNTs/GO/GCE sensor is displayed in Table 2. Azithromycin's antibacterial molecule concentration was ten times higher in the

presence of interference-causing compounds. We also display the recovery rate that was attained in the variation of the electrooxidation peak value of the azithromycin antibiotic molecules relative to the value of the electrooxidation peak of the azithromycin antibiotic molecules in the absence of the interferents with relative coefficients of variation (RSD) ranging from 4.33% to 5.22%.

Table 2. Influence of coexisting inorganic substances on the determination of 1.0×10^{-4} M Azithromycin (n = 3) by IL-TiO_2 NPs@MWCNTs/GO/GCE

Coexisting substance	Concentration de Coexisting substance (mmol L^{-1})	Change of peak current (%)	Coexisting substance	Concentration de Coexisting substance (mmol L^{-1})	Change of peak current (%)
Cl^-	1	-0 ,06	CO_3^{2-}	1	0,66
Fe^{3+}	1	-0, 12	Al^{3+}	1	-0,47
NO_3^-	1	-1,02	Ca^{2+}	1	-0,33
HCO3 –	1	-0.33	Cu^{2+}	1	-0,26
Ni^{2+}	1	-0,53	SO42-	1	-0,71
Pb2+	1	-0,07	Zn^{2+}	1	-0,40
K^+	1	0,04	Mg2+	1	-0,35

Following these tests, we discovered that the presence of various interfering substances did not significantly affect the determination of azithromycin antibiotic molecules. The signal recovery rate of electrocatalytic current and electrooxidation peak potential of azithromycin antibiotic molecules calculated were more than 91%. This demonstrates that the designed IL-TiO_2 NPs@MWCNTs/GO/GCE sensor has good selectivity and could be utilized to detect antibiotic compounds like azithromycin in real samples. Based on these findings, it can be concluded that the suggested method can be used to identify Azithromycin (AZT) in real samples and that when applied properly it works well.

3.8.4. Analytical application

By using the conventional addition approach, we examined the functionality of the created IL-TiO_2 -NPs@MWCNTs/GO/GCE electrode in real samples. Blood and human urine were two extremely distinct real samples that were selected. They received the same treatment before being heavily spiked with the antibiotic azithromycin to achieve concentrations of 10 µM, 5 µM, and 1 µM of human blood and urine, respectively. Each solution was examined by the IL-

TiO_2 -NPs@MWCNTs/GO/GCE sensor in accordance with the experimental protocol depicted in the diagram. DPV measurements were carried out as previously mentioned (Scheme 2).

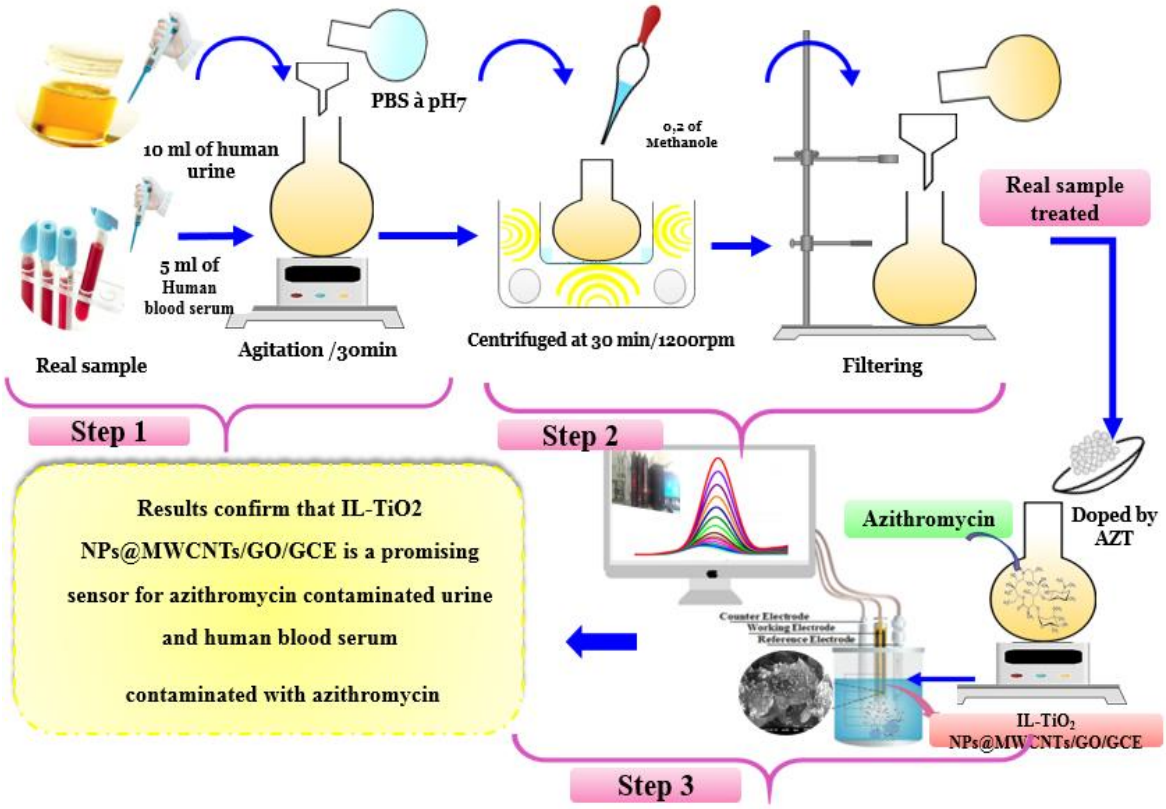

Scheme 2. Experimental protocol

Tableau 3. The recovery rate and coefficient of variation (RSD) of the sensor IL-TiO_2-NPs@MWCNTs/GCE in detecting the antibiotic azithromycin in actual human blood and urine samples. ND is not detected.

Sample	Spiked (µM)	Found (µM)	Accuracy (%)	RSD% (n=3)
Human blood	**0**	**ND**	**-**	**-**
	10	**9.66**	**96.6**	**3.2**
	5	**4.89**	**98.7**	**3.1**
	1	**0.942**	**94.2**	**2.8**
Human urine	**0**	**ND**	**-**	**-**
	10	**9.91**	**99.1**	**2.65**
	5	**4.9**	**98**	**2.43**
	1	**0.963**	**96.3**	**2.54**

Relative coefficients of variation (RSD) for the data in Table 3 range from 4.2% to 51%, with recoveries between 96.6% and 99.1%. Hence, we came to the conclusion that the created IL-TiO_2-NPs@MWCNTs/GCE sensors are sufficient for the identification of antibiotic residues in a real matrix, such as human urine and blood.

4. CONCLUSION

In this study, the developed IL-TiO_2-NPs@MWCNTs/GCE sensor was applied to the detection of azithromycin by the standard addition method in a human urine and blood sample certified with azithromycin antibiotics. The DPV measurements were performed as previously described. detection limit, calibration curve, sensitivity and selectivity were presented. the results obtained, showing the recovery rate ranging from 96.5% and 99.1%, with relative coefficients of variation (RSD) between 2.46% and 3.2%. we concluded that the developed IL-TiO_2-NPs@MWCNTs/GO/GCE sensors are adequate for the determination of azithromycin residues in a real matrix such as human urine and certified blood. The proposed electrochemical sensor exhibits excellent catalytic activity for the oxidation of the electroactive centers of azithromycin and provides a larger electroactive surface area and lower charge transfer resistance compared to MWCNTs/GCE. The transfer processes of azithromycin molecules are controlled by diffusion. The results show that the peak currents generated by these interferents are negligible compared to those of the target molecules. This phenomenon reveals the sensitivity of the response of the developed sensors, even in the presence of interfering compounds. The peak current and azithromycin concentration show a linear relationship in two ranges with a detection limit of 1.772×10^{-8} M and a quantification limit of 5.83×10^{-8} M. This new sensor has important and desirable advantages, such as fast response time, simplicity and significant cost reduction for the analysis of real samples contaminated with azithromycin.

Declarations of interest

The authors declare that they have no known competing financial interests or personal relationships that might appear to influence the work presented in this article. The authors declare no conflict of interest in this reported work.

REFERENCES

[1] M. Cochin, F. Touret, J.S. Driouich, G. Moureau, P.R. Petit, C. Laprie, C. Solas, X. de Lamballerie, and A. Nougairède, Antiviral Res. 197 (2022) 105212.

[2] L. Dong, S. Hu, and J. Gao, DD & T 14 (2020) 58.

[3] P. Gautret, J.C. Lagier, P. Parola, V.T. Hoang, L. Meddeb, M. Mailhe, B. Doudier, J. Courjon, V. Giordanengo, V.E. Vieira, H. Tissot Dupont, S. Honoré, P. Colson, E.

Chabrière, B. La Scola, J.-M. Rolain, P. Brouqui, and D. Raoult, Int. J. Antimicrobial Agents 56 (2020) 105949.
[4] D. Cucinotta, and M. Vanelli, Acta Bio Medica Atenei Parmensis 91 (2020) 157.
[5] G.W. Amsden, J. Antimicrobial Chemother. 55 (2005) 10.
[6] A. Elavarasi, M. Prasad, T. Seth, R.K. Sahoo, K. Madan, N. Nischal, M. Soneja, A. Sharma, S.K. Maulik, Shalimar, and P. Garg, J. Gen. Intern. Med. 35 (2020) 3308.
[7] A. Lacout, P.Y. Marcy, and C. Perronne, J. Gen. Intern. Med. 36 (2021) 2466.
[8] T. Rouamba, H. Barry, E. Ouédraogo, M.C. Tahita, N.V. Yaméogo, A. Poda, E.A. Diendéré, A.-S. Ouedraogo, I. Valea, A.M. Koné, C. Thiombiano, I. Traoré, Z. Tarnagda, S.A. Sawadogo, Z. Gansané, Y. Kambiré, I. Sanou, F. Barro-Traoré, M.K. Drabo, and H. Tinto, TCRM 17 (2021) 1187.
[9] P. Zarogoulidis, N. Papanas, I. Kioumis, E. Chatzaki, E. Maltezos, and K. Zarogoulidis, Eur. J. Clin. Pharmacol. 68 (2012) 479.
[10] M. Iannetta, G. Ippolito, E. Nicastri, Antimicrob Agents Chemother. 61 (2017) e01152.
[11] I.-A. Stoian, B.C. Iacob, C.L. Dudaș, L. Barbu-Tudoran, D. Bogdan, I.O. Marian, E. Bodoki, and R. Oprean, Biosens. Bioelectron. 155 (2020) 112098.
[12] A. Schögler, B.S. Kopf, M.R. Edwards, S.L. Johnston, C. Casaulta, E. Kieninger, A. Jung, A. Moeller, T. Geiser, N. Regamey, and M.P. Alves, Eur. Respir J. 45 (2015) 428.
[13] J. Gao, Z. Tian, and X. Yang, BST 14 (2020) 72.
[14] P. Rebelo, J.G. Pacheco, M.N.D.S. Cordeiro, A. Melo, and C. Delerue-Matos, Anal. Methods 12 (2020) 1486.
[15] M. Langelot, L. Cellerin, and P. Germaud, Revue de Pneumologie Clinique. 62 (2006) 215.
[16] B. Wu, Y. Guo, H. Cao, Y. Zhang, L. Yu, and N. Jia, Sens. Actuators B 186 (2013) 219.
[17] J.Y. Peng, C.T. Hou, X.X. Liu, H.B. Li, and X.Y. Hu, Talanta 86 (2011) 227.
[18] R.W. Han, N. Zheng, Z.N. Yu, J. Wang, X.M. Xu, X.Y. Qu, S.L. Li, Y.D. Zhang, and J.Q. Wang, Food Chem. 181 (2015) 119.
[19] H. Mater Mahnashi, A.M. Mahmoud, A. Saad Alkahtani, and M.M. El-Wekil, Microchem. J. 163 (2021) 105925.
[20] A.A. Ensafi, A.R. Allafchian, and B. Rezaei, Colloids and Surfaces B 103 (2013) 468.
[21] R.A. Lee, A. Guyton, D. Kunz, G.R. Cutter, and C.J. Hoesley, J. Hospital Medicine 11 (2016) 15.
[22] C. Milito, F. Pulvirenti, F. Cinetto, V. Lougaris, A. Soresina, A. Pecoraro, A. Vultaggio, M. Carrabba, G. Lassandro, A. Plebani, G. Spadaro, A. Matucci, G. Fabio, R.M. Dellepiane, B. Martire, C. Agostini, D. Abeni, S. Tabolli, and I. Quinti, J. Allergy and Clinical Immunology 144 (2019) 584.
[23] J.C. Hancox, M. Hasnain, W.V.R. Vieweg, E.L.B. Crouse, and A. Baranchuk, Therapeutic Advances in Infection 1 (2013) 155.

[24] S. Jafari, M. Dehghani, N. Nasirizadeh, and M. Azimzadeh, J. Electroanal. Chem. 829 (2018) 27.
[25] J.L. Rufino, H.R. Pezza, and L. Pezza, Anal. Sci. 24 (2008) 871.
[26] C. Taninaka, H. Ohtani, E. Hanada, H. Kotaki, H. Sato, and T. Iga, J. Chromat. B 738 (2000) 405.
[27] A. Kwiecień, J. Krzek, and Ł. Biniek, J. Planar Chromat. 21 (2008) 177.
[28] R. Gandhi, C.L. Kaul, and R. Panchagnula, J. Pharm. Biomed. Anal. 23 (2000) 1073.
[29] A.R. Breier, C.V. Garcia, T.P. Oppe, M. Steppe, and E.E.S. Schapoval, J. Pharm. Biomed. Anal. 29 (2002) 957.
[30] B.M. Chen, Y.Z. Liang, X. Chen, S.G. Liu, F.L. Deng, and P. Zhou, J. Pharm. Biomed. Anal. 42 (2006) 480.
[31] M. Rachidi, J. Elharti, K. Digua, Y. Cherrah, and A. Bouklouze, Anal. Lett. 39 (2006) 1917.
[32] J. Zoubir, I. Bakas, and A. Assabbane, Nanotechnol. Environ. Eng. 6 (2021) 54.
[33] J. Zoubir, I. Bakas, S. Qourzal, M. Tamimi, and A. Assabbane, J. Appl. Electrochem. (2023).
[34] J. Zoubir, N. Bougdour, W.E. Hayaoui, C. Radaa, A. Idlahcen, A. Assabbane, and I. Bakas, Electrocatalysis (2022).
[35] Jallal. Zoubir, C. Radaa, N. Bougdour, A. Idlahcen, I. Bakas, and A. Assabbane, Materials Science for Energy Technologies 4 (2021) 177.
[36] J. Zoubir, C. Radaa, I. Bakas, M. Tamimi, S. Qourzal, and A. Assabbane, Carbon Lett. 33 (2023) 761.
[37] J. Zoubir, C. Radaa, N. Bougdour, A. Idlahcen, W. El Hayaoui, N. Tajat, W. El Mouhri, I. Nadif, S. Qourzal, M. Tamimi, and A. Assabbane, I. Bakas, J. Indian Chem. Soc. 99 (2022) 100590.
[38] J. Zoubir, I. Bakas, and A. Assabbane, Heliyon 7 (2021) e07542.
[39] M. Palomeque, and P. Ortiz, Talanta 72 (2007) 101
[40] B. Uslu, and S.A. Ozkan, Anal. Lett. 44 (2011) 2644.
[41] K. Zhang, L. Lu, Y. Wen, J. Xu, X. Duan, L. Zhang, D. Hu, and T. Nie, Anal. Chim. Acta 787 (2013) 50.
[42] M. Avramov-Ivic, S. Petrovic, P. Zivkovic, D. Mijin, and K. Drljevic, CI & CEQ 16 (2010) 111.
[43] F. Li, X. Jiang, J. Zhao, and S. Zhang, Nano Energy 16 (2015) 488.
[44] H. Zhang, X. Wang, N. Li, J. Xia, Q. Meng, J. Ding, and J. Lu, RSC Adv. 8 (2018) 34241.
[45] W.K. Jo, S. Kumar, M.A. Isaacs, A. Lee, and S. Karthikeyan, J. Applied Catalysis B 201 (2017) 159.
[46] Q.A. Yousif, K.M. Mahdi, and H.A. Alshamsi, Optik 219 (2020) 165294.

[47] R. Hidayat, S. Wahyuningsih, and G. Fadillah, Mater. Sci. Eng. B 286 (2022) 116083.
[48] Y. Seekaew, A. Wisitsoraat, D. Phokharatkul, and C. Wongchoosuk, Sens. Actuators B 279 (2019) 69.
[49] J.O. Olowoyo, M. Kumar, B. Singh, V.O. Oninla, J.O. Babalola, H. Valdés, A.V. Vorontsov, and U. Kumar, Carbon 147 (2019) 385.
[50] G.T.S. How, A. Pandikumar, H.N. Ming, L.H. Ngee, Sci. Rep. 4 (2014) 5044.
[51] A.A. Saeed, M.N. Abbas, W.F. El-Hawary, Y.M. Issa, and B. Singh, Biosensors 12 (2022) 778.
[52] S.D. Bukkitgar, and N.P. Shetti, Anal. Methods 9 (2017) 4387.
[53] N. Sun, J. Ma, C. Wang, J. Xue, L. Qiang, and J. Tang, Superlattices and Microstructures 121 (2018) 1.
[54] Q. He, J. Liu, X. Liu, G. Li, P. Deng, J. Liang, and D. Chen, Sensors 18 (2018) 1911.
[55] L. Bertel, D.A. Miranda, and J.M. García-Martín, Sensors 21 (2021) 6167.
[56] L.M. Pastrana-Martínez, S. Morales-Torres, V. Likodimos, P. Falaras, J.L. Figueiredo, J.L. Faria, and A.M.T. Silva, Applied Catalysis B 158 (2014) 329.
[57] D.K. Chouhan, T.U. Patro, G. Harikrishnan, S. Kumar, S. Gupta, G.S. Kumar, H. Cohen, and H.D. Wagner, Applied Clay Sci. 132–133 (2016) 105.
[58] J. Yu, T. Ma, S. Liu, Phys. Chem. Chem. Phys. 13 (2011) 3491.
[59] A.A. Kashale, K.P. Gattu, K. Ghule, V.H. Ingole, S. Dhanayat, R. Sharma, J.Y. Chang, and A.V. Ghule, Composites Part B 99 (2016) 297.
[60] E. Laviron, J. Electroanal. Chem. Inter. Electrochem. 100 (1979) 263.
[61] T. Zhou, Y. Tao, H. Jin, B. Song, T. Jing, D. Luo, Y. Zhou, Y. Zhou, Y.I. Lee, and S. Mei, PLoS One 11 (2016) e0147002.
[62] M.A. Abu-Dalo, N.S. Nassory, N.I. Abdulla, and I.R. Al-Mheidat, J. Electroanal. Chem. 751 (2015) 75.